Progress In Electromagnetics Research, Vol. 105, 119–139, 2010

BISTATIC SCATTERING FROM TWO-DIMENSIONAL DIELECTRIC OCEAN ROUGH SURFACE WITH A PEC OBJECT PARTIALLY EMBEDDED BY USING THE G-SMCG METHOD

W.-J. Ji and C.-M. Tong

Missile Institute
Air Force Engineering University
P. O. Box 25, Sanyuan, Shannxi 713800, China

Abstract—An efficient approach called general sparse matrix canonical grid (G-SMCG) method is proposed to analyze the electromagnetic scattering from 2-D dielectric rough surface with a conducting object partially buried. In this paper, the scattering of 3-D arbitrarily shaped object is computed by using the traditional method of moments (MoM) with RWG basis function, and the scattering of rough surface is analyzed by using the SMCG method. The coupling interactions between an object and rough surface are calculated by iterative method. Combing the ocean rough surface with Pierson_Moskowitz (PM) spectrum, the bistatic scattering coefficients of typical objects buried in the ocean surface have been computed by using the proposed method. Then the accuracy and efficiency of this method are discussed. Finally, the bistatic scattering coefficients of a ship located on ocean surface are calculated, and the influence of sea state and wind direction on the scattering coefficients is indicated.

1. INTRODUCTION

The electromagnetic (EM) scattering from objects located above or buried in a rough surface, which is applied to microwave sensing and radar signature widely, has been studied extensively using analytical and numerical methods in the past decades. In the actual applications, different objects are located in different environments. For example, ships are located on the sea, and tanks are located on the ground, which can be considered as objects partially buried in

Corresponding author: W.-J. Ji (jiweijie01@163.com).

rough surface. Hence, solutions for the electromagnetic scattering from partially buried objects are needed. However, more research has focused on the EM scattering from objects located entirely above or below a rough surface ([1–14]), and there are few publications on electromagnetic scattering from the partially embedded objects in dielectric rough surface between two media. For analyzing the electromagnetic scattering from a ship on ocean surface, not only should the electromagnetic scattering of targets and the rough surface be taken into account respectively, but also the coupling scattering field between them should be computed. Thus, more accurate model is required to study the effects of the rough surface on the object's scattering property.

In past researches, in order to use analytical method, the interface of the ground and ocean surface was usually assumed to be a planar interface or rough surface with small roughness limit ([10–14]). The advantage of the analytical method is the computational simplicity, but it only adapts to canonical geometries and a small rms rough surface height. Effect such as multiple scattering, shadowing and diffraction is very difficult to model analytically. Therefore, a numerical method has to be used to characterize the EM scattering from general target located on the rough surface. In order to numerically simulate the scattering from the object partially buried in rough surface, some fast numerical methods have been studied. The MoM and finite-difference method have been applied to analyzing the electromagnetic scattering from a 2-D PEC cylinder partially buried in flat dielectric interface. In [15–18], the scattering problem of a PEC cylinder partially buried in one-dimensional dielectric rough surface has been studied by using the MoM. In [19], the Generalized Forward-Backward Method (GFBM) is proposed to analyze the scattering from target on ocean-like rough surfaces. In [20], The GFBM/SAA is applied to numerical simulation of bistatic scattering from one-dimensional arbitrary dielectric constant soil surface with a conducting object partially buried under the tapered wave.

Different methods have been developed in recent years in order to reduce the number of computer operations required to analyze the rough surface scattering problem via the numerical method. It is worth mentioning, among others, that the sparse matrix canonical grid method (SMCG) [21–25] has been shown to be an extremely efficient method for the computation of scattering from 2-D dielectric rough surface, with the computational complexity of $O(N \log N)$ and memory requirement of $O(N)$. However, the SMCG fails to converge in the presence of a target (ship) on the rough surface mainly due to the strong interaction between the obstacle and ocean-like surface.

What is more, in the conventional formulation involved in the standard SMCG method, it does not take the interaction within the obstacle itself into account. In this paper, we propose an efficient approach to analyze the electromagnetic scattering from conducting object partially buried in 2-D dielectric rough surface (3-D scattering problem). The scattering of 3-D arbitrarily shaped object is computed by using the traditional method of moments (MoM) with RWG basis function [26], and the scattering of rough surface is analyzed by using the SMCG method. A numerical iterative method is used to calculate the coupling interactions between object and surface. As a conclusion, we call this method general sparse matrix canonical grid method (G-SMCG). The computational cost of the G-SMCG method is essentially the same as the conventional SMCG method since the direct matrix size is usually fixed for the finite sized target which is smaller than the rough surface.

As numerical examples, the EM scattering from typical objects partially buried in ocean surface with PM spectrum are calculated using G-SMCG, and the accuracy and efficiency of this method are discussed. At last, with different directions of incident waves, the bistatic scattering coefficients of a PEC ship located on ocean surface are computed. Additionally, the influence of sea state and wind direction on the scattering coefficients is also indicated.

2. THEORY AND FORMULATION

Consider a perfect conducting object partially buried in 2-D dielectric rough surface as shown in Fig. 1, where the rough surface is described by $z = f(x, y)$, generated by Monte Carlo method. The top and bottom regions are half spaces, and the dielectric constants are ε_0 and ε_1. The permeability of all layers is assumed to be μ_0.

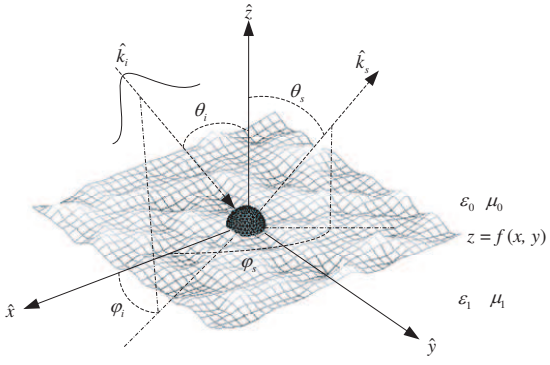

Figure 1. Geometry of a PEC object partially buried in 2-D dielectric rough surface.

2.1. The Coupling Interaction Integral Equations

In practical cases, the incident field is tapered so that the illuminated rough surface can be confined to the surface area $L_x \times L_y$. Assume the tapered plane wave incident on the structure along $\hat{\mathbf{k}}_i = \sin\theta_i \cos\phi_i \hat{\mathbf{x}} + \sin\theta_i \sin\phi_i \hat{\mathbf{y}} - \cos\theta_i \hat{\mathbf{z}}$, which is the incident wave vector. The incident fields can be expressed in terms of spectrum of the incident wave [22]

$$\mathbf{H}^{inc}(x,y,z) = -\frac{1}{\eta}\int_{-\infty}^{\infty} dk_x \int_{-\infty}^{\infty} dk_y \exp(ik_x x + ik_y y - ik_z z) \cdot E_{TE}(k_x,k_y)\hat{\mathbf{h}}(-k_z) \tag{1}$$

$$\mathbf{E}^{inc}(x,y,z) = \int_{-\infty}^{\infty} dk_x \int_{-\infty}^{\infty} dk_y \exp(ik_x x + ik_y y - ik_z z) \cdot E_{TE}(k_x,k_y)\hat{\mathbf{e}}(-k_z) \tag{2}$$

$$\text{where } E_{TE}(k_x,k_y) = \frac{1}{4\pi^2}\int_{-\infty}^{\infty} dx \int_{-\infty}^{\infty} dy \exp(-ik_x x - ik_y y) \cdot \exp(i(k_{ix}x + k_{iy}y)(1+w)) \exp(-t) \tag{3}$$

$$t = t_x + t_y = (x^2+y^2)/g^2 \tag{4}$$

$$t_x = \frac{(\cos\theta_i \cos\varphi_i x + \cos\theta_i \sin\varphi_i y)^2}{g^2 \cos^2\theta_i} \tag{5}$$

$$t_y = \frac{(-\sin\phi_i x + \cos\phi_i y)^2}{g^2} \tag{6}$$

$$w = \frac{1}{k_0}\left[\frac{(2t_x - 1)}{g^2\cos^2\theta_i} + \frac{(2t_y-1)}{g^2}\right] \tag{7}$$

The parameter g controls the tapering of the incident wave.

For TE wave incidence

$$\hat{\mathbf{e}}(-k_z) = \frac{1}{k_\rho}(\hat{\mathbf{x}}k_y - \hat{\mathbf{y}}k_x) \tag{8}$$

$$\hat{\mathbf{h}}(-k_z) = \frac{k_z}{k_0 k_\rho}(\hat{\mathbf{x}}k_x - \hat{\mathbf{y}}k_y) + \frac{k_\rho}{k_0}\hat{\mathbf{z}} \tag{9}$$

And for TM wave incidence

$$\hat{\mathbf{h}}(-k_z) = -\frac{1}{k_\rho}(\hat{\mathbf{x}}k_y - \hat{\mathbf{y}}k_x) \tag{10}$$

$$\hat{\mathbf{e}}(-k_z) = \frac{k_z}{k_0 k_\rho}(\hat{\mathbf{x}}k_x - \hat{\mathbf{y}}k_y) + \frac{k_\rho}{k_0}\hat{\mathbf{z}} \tag{11}$$

with $k_z = \sqrt{k_0^2 - k_\rho^2}$ and $k_\rho = \sqrt{k_x^2 + k_y^2}$. In the above k_0 and η are the wave-number and wave impedance of free space respectively, and $\hat{\mathbf{e}}$, $\hat{\mathbf{h}}$ denote the polarization vectors.

Let $\mathbf{r}' = x'\hat{\mathbf{x}} + y'\hat{\mathbf{y}} + f(x', y')\hat{\mathbf{z}}$ denote a source point, and $\mathbf{r} = x\hat{\mathbf{x}} + y\hat{\mathbf{y}} + f(x, y)\hat{\mathbf{z}}$ denote a field point. If there is no object buried in the rough surface, the surface fields satisfy the following boundary integral equations

$$\frac{\hat{\mathbf{n}} \cdot \mathbf{E}_s(\mathbf{r})}{2} - \hat{\mathbf{n}} \cdot \left\{ \int_S \hat{\mathbf{n}}' \times \mathbf{H}_s(\mathbf{r}') i\omega\mu G_0 ds' + P \int_S [(\hat{\mathbf{n}}' \times \mathbf{E}_s(\mathbf{r}')) \times \nabla' G_0 + \hat{\mathbf{n}}' \cdot \mathbf{E}_s(\mathbf{r}') \nabla' G_0] ds' \right\} = \hat{\mathbf{n}} \cdot \mathbf{E}^{inc}(\mathbf{r}) \quad (12)$$

$$\frac{\hat{\mathbf{n}} \times \mathbf{H}_s(\mathbf{r})}{2} - \hat{\mathbf{n}} \times \left\{ \int_S (-i\omega) \hat{\mathbf{n}}' \times \mathbf{E}_s(\mathbf{r}') \varepsilon_0 G_0 ds' + P \int_S [(\hat{\mathbf{n}}' \times \mathbf{H}_s(\mathbf{r}')) \times \nabla' G_0 + \hat{\mathbf{n}}' \cdot \mathbf{H}_s(\mathbf{r}') \nabla' G_0 ds' \right\} = \hat{\mathbf{n}} \times \mathbf{H}^{inc}(\mathbf{r}) \quad (13)$$

$$-\frac{\hat{\mathbf{n}} \times \mathbf{E}_s(\mathbf{r})}{2} - \hat{\mathbf{n}} \times \left\{ \int_S \hat{\mathbf{n}}' \times \mathbf{H}_s(\mathbf{r}') i\omega\mu G_1 ds' + P \int_S [(\hat{\mathbf{n}}' \times \mathbf{E}_s(\mathbf{r}')) \times \nabla' G_1 + \hat{\mathbf{n}}' \cdot \mathbf{E}_s(\mathbf{r}') \nabla' G_1] ds' \right\} = 0 \quad (14)$$

$$-\frac{\hat{\mathbf{n}} \cdot \mathbf{H}_s(\mathbf{r})}{2} - \hat{\mathbf{n}} \cdot \left\{ \int_S (-i\omega) \hat{\mathbf{n}}' \times \mathbf{E}_s(\mathbf{r}') \varepsilon_1 G_1 ds' + P \int_S [(\hat{\mathbf{n}}' \times \mathbf{H}_s(\mathbf{r}')) \times \nabla' G_1 + \hat{\mathbf{n}}' \cdot \mathbf{H}_s(\mathbf{r}') \nabla' G_1] ds' \right\} = 0 \quad (15)$$

where S denotes the rough surface. $\mathbf{E}_s$ and $\mathbf{H}_s$ are the surface fields of the rough surface, and the integral $P\int$ denote a Cauchy integral. G_0 is the three-dimensional Green's function of free space, and G_1 is the three-dimensional Green's function of lower dielectric medium. They are given by

$$G_{0,1} = \frac{\exp(ik_{0,1}R)}{4\pi R}$$

where $R = \sqrt{(x - x')^2 + (y - y')^2 + (f(x, y) - f(x', y'))^2}$ and k_1 is the wave-number of the lower medium. The unit normal vectors $\hat{\mathbf{n}}$ and $\hat{\mathbf{n}}'$ refer to primed coordinates and point away from the lower medium.

If there is only the PEC object in free-space, the fields satisfy the following boundary integral equations

$$\mathbf{E}^{inc}(\mathbf{r})\big|_{\tan} = i\omega\mu_0 \int_{S_b} [\hat{\mathbf{n}}_b' \times \mathbf{H}_b(\mathbf{r}') + \frac{1}{k_0^2} \nabla(\nabla' \cdot (\hat{\mathbf{n}}_b' \times \mathbf{H}_b(\mathbf{r}')))] G_0 ds' \quad (16)$$

where S_b denotes the surface of object. $\mathbf{H}_b$ are the surface fields of the object, and $\hat{\mathbf{n}}_b'$ refer to primed coordinate and point away from the object.

When there are both object and rough surface, the coupling interaction between them must been considered. The scattering fields of object can be calculated by following formulas [24]

$$\mathbf{H}_b^s(\mathbf{r}) = \int_{S_b} \mathbf{J}_b(\mathbf{r}') \times \nabla' G_q ds' \tag{17}$$

$$\mathbf{E}_b^s(\mathbf{r}) = -\frac{i}{\omega\varepsilon_q} \nabla \times \int_S \mathbf{J}_b(\mathbf{r}') \times \nabla' G_q(\mathbf{r}, \mathbf{r}') ds' \tag{18}$$

where $\mathbf{J}_b(\mathbf{r}) = \hat{\mathbf{n}}_b \times \mathbf{H}_b(\mathbf{r})$, $q = 0, 1$ denote the scatter fields of object in free space and lower medium, respectively.

The scattering fields from rough surface to object can be calculated by following method [24]

$$\mathbf{E}_S^s(\mathbf{r}) = -\int_S [(-i\omega\mu_q)\mathbf{J}_S(\mathbf{r}')G_q + \mathbf{M}_S(\mathbf{r}') \times \nabla' G_q + \nabla' G_q \hat{\mathbf{n}}' \cdot \mathbf{E}_S(\mathbf{r}')] ds' \tag{19}$$

where $\mathbf{M}_S(\mathbf{r}) = \hat{\mathbf{n}} \times \mathbf{E}_S(\mathbf{r})$ and $\mathbf{J}_S(\mathbf{r}) = \hat{\mathbf{n}} \times \mathbf{H}_S(\mathbf{r})$, $q = 0, 1$ denote the scatter fields from rough surface to object in free space and lower medium, respectively.

In summary, the total equations for PEC object partially buried in dielectric rough surface are

$$\frac{\hat{\mathbf{n}} \cdot \mathbf{E}_s(\mathbf{r})}{2} - \hat{\mathbf{n}} \cdot \left\{ \int_S \mathbf{J}_s(\mathbf{r}') i\omega\mu G_0 ds' + P \int_S [\mathbf{M}_s(\mathbf{r}') \times \nabla' G_0 + \hat{\mathbf{n}} \cdot \mathbf{E}_s(\mathbf{r}') \nabla' G_0] ds' \right\} = \hat{\mathbf{n}} \cdot (\mathbf{E}^{inc}(\mathbf{r}) + \mathbf{E}_b^s(\mathbf{r})) \tag{20}$$

$$\frac{\mathbf{J}_s(\mathbf{r})}{2} - \hat{\mathbf{n}} \times \left\{ \int_S (-i\omega)\mathbf{M}_s(\mathbf{r}')\varepsilon_0 G_0 ds' + P \int_S [(\mathbf{J}_s(\mathbf{r}')) \times \nabla' G_0 + \hat{\mathbf{n}} \cdot \mathbf{H}_s(\mathbf{r}') \nabla' G_0 ds' \right\} = \hat{\mathbf{n}} \times (\mathbf{H}^{inc}(\mathbf{r}) + \mathbf{H}_b^s(\mathbf{r})) \tag{21}$$

$$-\frac{\mathbf{M}_s(\mathbf{r})}{2} - \hat{\mathbf{n}} \times \left\{ \int_S \mathbf{J}_s(\mathbf{r}') i\omega\mu G_1 ds' + P \int_S [(\mathbf{M}_s(\mathbf{r}')) \times \nabla' G_1 + \hat{\mathbf{n}} \cdot \mathbf{E}_s(\mathbf{r}') \nabla' G_1] ds' \right\} = -\hat{\mathbf{n}} \times \mathbf{E}_b^s(\mathbf{r}) \tag{22}$$

$$-\frac{\hat{\mathbf{n}} \cdot \mathbf{H}_s(\mathbf{r})}{2} - \hat{\mathbf{n}} \cdot \left\{ \int_S (-i\omega)\mathbf{M}_s(\mathbf{r}')\varepsilon_1 G_1 ds' + P \int_S [(\mathbf{J}_s(\mathbf{r}')) \times \nabla' G_1 + \hat{\mathbf{n}}' \cdot \mathbf{H}_s(\mathbf{r}') \nabla' G_1] ds' \right\} = -\hat{\mathbf{n}} \cdot \mathbf{H}_b^s(\mathbf{r}) \tag{23}$$

$$(\mathbf{E}^{inc}(\mathbf{r}) + \mathbf{E}_S^s(\mathbf{r}))\big|_{\tan} = i\omega\mu_0 \int_{S_b} \left[\mathbf{J}_b(\mathbf{r}') + \frac{1}{k_q^2} \nabla(\nabla' \cdot (\mathbf{J}_b(\mathbf{r}'))) \right] G_q ds' \tag{24}$$

The MoM is used to discretize the integral Equations (20)–(24). If we solve the equations using traditional method such as Gaussian elimination directly, the number of unknowns is very enormous; the complexity is $O(N^3)$; it will be very time-consuming. So fast numerical method must been introduced.

2.2. The General Sparse Matrix Canonical Grid Method (G-SMCG)

Although the surface of object is close, it can be detached from the rough dielectric surface into two parts. One of witch is above the surface, and the other is below the surface, as shown in Fig. 2.

So both the object and rough surface have been divided into three parts. Part 1 is dielectric rough surface, which is Section 1 in Fig. 2. Part 2 is perfect conducting object surface above rough surface, which is Section 2 in Fig. 2. Part 3 is the object surface below rough surface, which is Section 3 in Fig. 2.

The integral equations of Section 1 is discretized by using MoM with pulse base function. Therefore, the integral equations of Section 2 and Section 3 are discretized by using MoM with RWG base function. Then we get the following matrix equation

$$\mathbf{Z}^{total}\mathbf{I}^{total} = \mathbf{V}^{inc} \tag{25}$$

where the impendence matrix $\mathbf{Z}^{total}$ is for both rough surface and object, and $\mathbf{I}^{total}$ is the unknown vector of both rough surface and object. $\mathbf{V}^{inc}$ is the total initialized incident vector. The number of the unknowns for 2-D dielectric rough surface is always thousands upon thousands. So it is time consuming and difficult to solve this equation using traditional MoM. We adopt the following fast method to solve this equation.

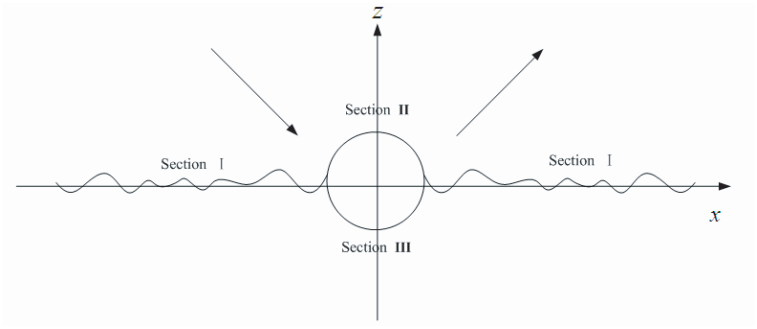

Figure 2. Geometry of three sections.

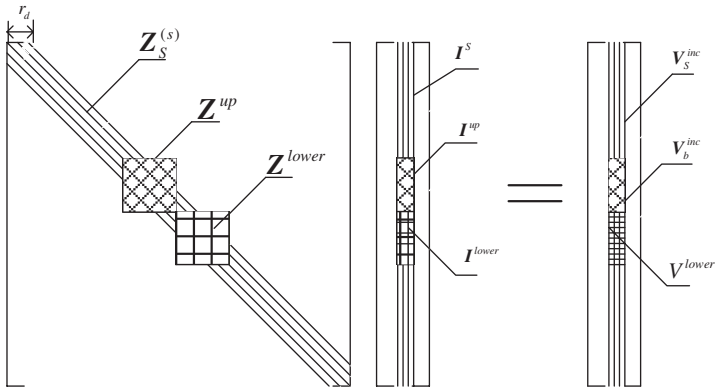

Figure 3. Geometry of matrix.

The equations for rough surface are also solved using traditional SMCG as follows. We choose a neighborhood distance r_d as the distance which defines the boundary between the weak and strong elements of the impedance matrix. Then the impedance matrix is decomposed into the sum of a strong matrix $\mathbf{Z}_S^{(s)}$ and a weak matrix $\mathbf{Z}_S^{(w)}$.

$$\mathbf{Z}_S = \mathbf{Z}_S^{(s)} + \mathbf{Z}_S^{(w)} \tag{26}$$

where $\mathbf{Z}_S^{(s)}$ represents near field strong interaction, and $\mathbf{Z}_S^{(w)}$ represents non-near field weak interaction. The weak matrix elements are expanded in a Taylor's series about the horizontal distance between the two points

$$\mathbf{Z}_S^{(w)} = \sum_{m=0}^{M} \mathbf{Z}_m^{(w)} \tag{27}$$

The zeroth term in (27) is called the flat surface contribution.

$$\mathbf{Z}_S^{(FS)} = \mathbf{Z}_0^{(w)} \tag{28}$$

Then the equations are solved using iterative method as the conjugate gradient method (CGM). The matrix-vector products of $\mathbf{Z}_S^{(FS)}\mathbf{I}_S$ and $\mathbf{Z}_m^{(w)}\mathbf{I}_S$ can be computed using a 2-D FFT algorithm. However, the equation for PEC object is solved using traditional MoM. We call this method G-SMCG.

As a result, the structure of impendence matrix $\mathbf{Z}^{total}$ is shown in Fig. 3. $\mathbf{Z}_S^{(s)}$ is the strong interaction matrix of rough surface. $\mathbf{Z}^{up}$ and $\mathbf{Z}^{lower}$ are the impedance matrix of Section 2 and Section 3

respectively. The width of the half band is r_d. $\mathbf{I}^S$ is the unknown vector of rough surface. $\mathbf{I}^{up}$ and $\mathbf{I}^{lower}$ are the unknown vectors of Section 2 and Section 3 respectively. $\mathbf{V}_S^{inc}$ and $\mathbf{V}_b^{inc}$ are the incident vectors of rough surface and Section 2 respectively. It should be noted that the initialized incident vector of Section 3 is zero.

The total steps of G-SMCG as follows

STEP1. Solve the equations of rough surface by using SMCG.

$$\left(\mathbf{Z}_S^{(s)} + \mathbf{Z}^{(FS)}\right)\mathbf{J}_S^{(1)} = \mathbf{b} \tag{29}$$

$$\left(\mathbf{Z}_S^{(s)} + \mathbf{Z}^{(FS)}\right)\mathbf{J}_S^{(i+1)} = \mathbf{b}^{(i+1)} \tag{30}$$

$$\mathbf{b}^{(i+1)} = \mathbf{b} - \sum_{m=1}^{M} \mathbf{Z}_m^{(w)}\mathbf{J}_S^{(i)} \tag{31}$$

Equations (29) and (30) are solved using CGM. The matrix-vector products of $\mathbf{Z}_S^{(FS)}\mathbf{J}_S$, and $\mathbf{Z}_m^{(w)}\mathbf{J}_S$ are computed using a 2-D FFT algorithm. We keep the expansion terms at $6(M = 5)$.

STEP2. Calculate the scattering field $\mathbf{E}_S^s$, which comes from rough surface to object by solving formula (19).

STEP3. Solve the equations of object by using MoM with RWG base function.

$$\mathbf{Z}^{T\arg et}\mathbf{J}_b = \mathbf{V}_b^{inc} + \mathbf{E}_S^s \tag{32}$$

Here, the scattering field from rough surface has been taken into consideration. Because the object size is much smaller than the rough surface, $\mathbf{V}_b^{inc}$ is considered as plane incident wave.

STEP4. Calculate the scattering field $\mathbf{H}_b^s$ and $\mathbf{E}_b^s$, witch come from object to rough surface by solving formulas (17) and (18).

STEP5. Calculate the relative error. The iteration is terminated when the relative error is less than the appointed precision. Otherwise, go back to STEP1 after updating the incidence vector of rough surface.

$$\mathbf{b}^{(0)} = \mathbf{V}_{inc}^S + \mathbf{V}_b^s \tag{33}$$

where $\mathbf{V}_b^s$ contains $\mathbf{H}_b^s$ and $\mathbf{E}_b^s$.

Defining the relative error at the nth iteration as

$$\tau(n) = \frac{\left|\mathbf{Z}^{total}(\mathbf{I}^{total,(n)} - \mathbf{I}^{total,(n-1)})\right|}{|\mathbf{V}^{inc}|} \tag{34}$$

where the $\mathbf{I}^{total,(n)}$ and $\mathbf{I}^{total,(n-1)}$ are the unknown vectors at nth and $n-1$th iteration. The computational complexity of the G-SMCG is $O(N^{Sur}\log N^{Sur} + (N^{Tar})^2)$. Assume that the number of surface unknowns N^{Sur} is much larger than the number of target

unknowns N^{Tar}, the computational complexity of G-SMCG can be considered as $O(N^{Sur}\log N^{Sur})$. This is true for most problems of interest, which usually involve an obstacle which is much smaller than the very large ocean surface on which it is situated. The storage requirement is $O(N^{Sur})$ to store the strong matrix of ocean surface, with the additional storage of a matrix of size $N^{Tar}\times N^{Tar}$. Thus the computational complexity and memory requirements for the G-SMCG method are practically the same as the conventional SMCG method.

This method is an accurate numerical approach for PEC object partially buried in 2-D dielectric rough surface. All of the multiple interactions are taken into consideration in this solution. With the complexity of almost $O(N^{Sur}\log N^{Sur})$, this method is a very fast numerical method. As a conclusion, we call this method G-SMCG.

2.3. The Bistatic Scattering Coefficient

Numerical results are presented in terms of the normalized bistatic scattering coefficient $\sigma_{\alpha\beta}(\theta_s,\phi_s,\theta_i,\varphi_i)$, defined for a scattered wave in α-polarization and an incident wave in β-polarization as

$$\sigma_{\alpha\beta}(\theta_s,\varphi_s,\theta_i,\varphi_i)=\lim_{r\to\infty}\frac{4\pi r^2\left|E_\alpha^{Sur}+E_\alpha^{up,Tar}\right|^2}{2\eta\int_S\mathbf{S}_\beta^i\cdot\hat{\mathbf{n}}ds} \tag{35}$$

where $\mathbf{E}_\alpha^{Sur}$ is the α-polarized scattered field of rough surface, and $\mathbf{E}_\alpha^{up,Tar}$ is the α-polarized scattered field of Section 2, and

$$\begin{aligned}
E_h^{Sur} &= \frac{ik_0}{4\pi r}\exp(-ikr)\int_S[(M_{sx}\cos\theta_s\cos\varphi_s+M_{sy}\cos\theta_s\sin\varphi_s\\
&\quad -M_{sz}\sin\theta_s)-\eta(J_{sx}\sin\varphi_s-J_{sy}\cos\varphi_s)]\,ds\\
E_v^{Sur} &= \frac{ik_0}{4\pi r}\exp(-ikr)\int_S[(M_{sx}\sin\varphi_s-M_{sy}\cos\varphi_s)\\
&\quad +\eta(J_{sx}\cos\theta_s\cos\varphi_s+J_{sy}\cos\theta_s\sin\varphi_s-J_{sz}\sin\theta_s)]\,ds\\
E_h^{up,Tar} &= \frac{\eta ik_0}{4\pi r}\exp(-ikr)\int_{S_{up}}(J_{bx}\sin\varphi_s-J_{by}\cos\varphi_s)ds\\
E_v^{up,Tar} &= \frac{\eta ik_0}{4\pi r}\exp(-ikr)\int_{S_{up}}(-J_{bx}\cos\theta_s\cos\varphi_s\\
&\quad -J_{by}\cos\theta_s\sin\varphi_s+J_{bz}\sin\theta_s)ds
\end{aligned}$$

where $\mathbf{S}_\beta^i$ is the time average Poynting vector of the β-polarized incident wave. S_{up} is the surface of Section 2, and S is the 2-D rough surface profile of interest.

3. NUMERICAL RESULTS AND DISCUSSIONS

In this section, several examples are presented using the proposed method, in which a ocean rough surface is generated as a zero-mean Gaussian random process with the PM wave spectrum [27]

$$W_{PM}(k,\varphi) = \frac{a_0}{2K^4}\exp\left(-\frac{\beta g_0^2}{K^2 U_{19.5}^4}\right)\Phi(\varphi) \tag{36}$$

where

$$\Phi(\varphi) = \frac{\cos^2(\varphi-\varphi_v)}{\pi}$$
$$K = \sqrt{k_x + k_y}$$
$$\varphi = \tan^{-1}(k_y/k_x)$$

thus (36) can be rewritten as

$$W_{PM}(k_x,k_y) = \frac{a_0}{2(k_x^2+k_y^2)^2}\exp\left(-\frac{\beta g^2}{(k_x^2+k_y^2)U_{19.5}^4}\right) \cdot \frac{\cos^2(\tan^{-1}(k_y/k_x)-\varphi_v)}{\pi} \tag{37}$$

The rms height of ocean surface is $h^2 = a_0 U_{19.5}^4/4\beta g^2$. Here, $a_0 = 0.0081$, $\beta = 0.74$, g_0 is the gravitational acceleration equal to 9.81 m/s, and $U_{19.5}$ is the wind speed, in m/s, at the altitude of 19.5 meter above the mean ocean level. ϕ_v is the direction of wind, and $\phi_v = 0$ denotes the direction is $\hat{\mathbf{x}}$. The main characteristics of the PM spectrum are that higher wind speeds give rise to longer ocean waves (lower wavenumber), whereas the small-scale waves (higher wavenumber) are relatively unaffected by the wind speed.

3.1. Validation of the Computations

In the following examples, the size of the rough surface is $8\lambda \times 8\lambda$. $U_{19.5} = 5\,\text{m/s}$, $\phi_v = 0$, and the rms height of the ocean surface is $h = 0.1334\,\text{m}$. The relative permittivity of the sea-water is $\varepsilon_r = 2.0 + 0.2i$. The surface is sampled at 64 points per λ^2 giving 4096 points on the rough surface and 24576 surface unknowns. The neighborhood distance in the implementation of G-SMCG is $r_d = 2.5\lambda$. A tapered wave is incident from the direction of $\theta_i = 30°$, and $\varphi = 0°$ direction. Working frequency is 300 MHz. The G-SMCG method is implemented on a personal computer with Pentium(R) Dual-core CPU. For CPU: 2.5 GHz; Memory: 2 GB. The numerical results presented in the following are the average of 10 Monte Carlo realizations. Because

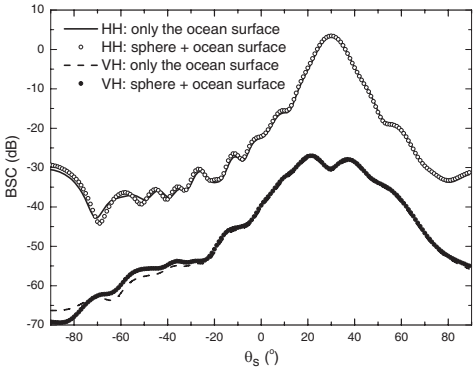

Figure 4. The validation of the computation ($\varphi_s = \varphi_i = 0°$).

of the limit of paper length, we only compute the EM scattering for H-polarization incidence wave. However, the EM scattering for V-polarization incidence wave can be calculated by using the same method.

The numerical simulation is conducted for a perfectly electrical conductor (PEC) sphere buried under a 2-D ocean rough surface as shown in Fig. 1. The center of the sphere is at $z = 0$ plane. The radius of sphere is $a = 0.01\lambda$. The error norm criterion is set at $< 1\%$. Making the average of 10 realizations, bistatic HH and VH-polarized scattering coefficients (BSC) are computed using the G-SMCG shown in Fig. 4. The BSC of only 2-D rough surface with the same parameter using the traditional SMCG are also presented to validate the proposed method. From Fig. 4, we clearly see that two results match very well for nearly all angles.

3.2. Discuss

Figure 5(a) shows the BSC of sphere with radius $a = 0.3\lambda$ partially buried in 2-D ocean surface for both HH and VH-polarizations. Azimuthal variation of bistatic HH and VH-polarized scattering coefficients are shown in Fig. 5(b). The ocean surface and incident wave are the same as those described in Section 3.1. The surface of the sphere is discretized into 365 triangle patches. In order to illustrate the rough surface effect, we also compute the BSC of rough surface without object with the same parameter. From Fig. 5, the peak value appears at $\theta_s = 30°$. It can be seen that co-polarized scattering is always stronger than cross-polarized at most scattering angles, and scattering peaks occur at $\theta_s = 30°$ for both polarizations. When an object is partially buried in ocean surface, HH-polarized scattering is greatly enhanced, and HV-polarized scattering is also uniformly increased due to the object presence.

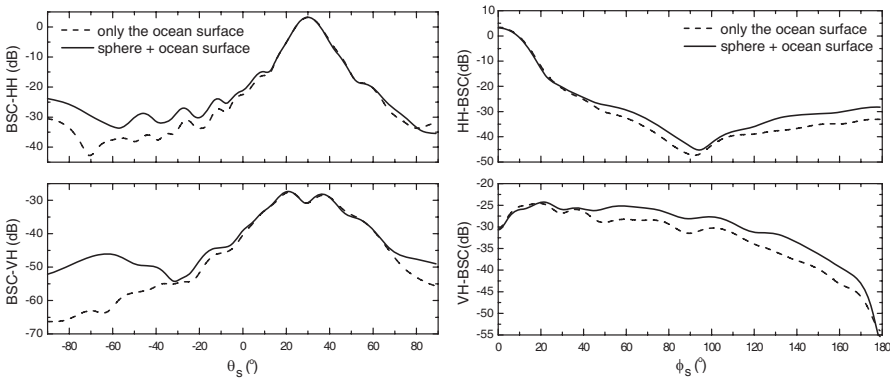

Figure 5. Sphere partially buried in ocean surface ($\varphi_i = 0°$).

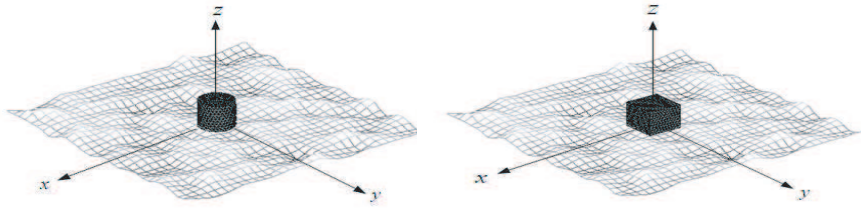

Figure 6. Geometry of targets located on ocean surface.

In the second example, the target is a cylinder with radii of 0.3λ and height 0.6λ. The ocean surface and incident wave are the same as those described earlier. The surface of cylinder is discretized into 578 triangle patches. In the third example, a cube with dimensions $0.6\lambda \times 0.6\lambda \times 0.6\lambda$ is partially buried in ocean surface, and the surface of cube is discretized into 666 triangle patches. The centers of the cylinder and cube are both at $z = 0$ plane as shown in Fig. 6.

Figures 7 and 8 show the BSC for the second and third examples, respectively. As expected, the bigger the object is, the more obvious the change of BSC is. Because the object's size is much smaller than the ocean surface, angular pattern of total bistatic scattering seems to be governed by ocean surface scattering. The difference between the cases with and without the object can show the scattering effect due to the object presence.

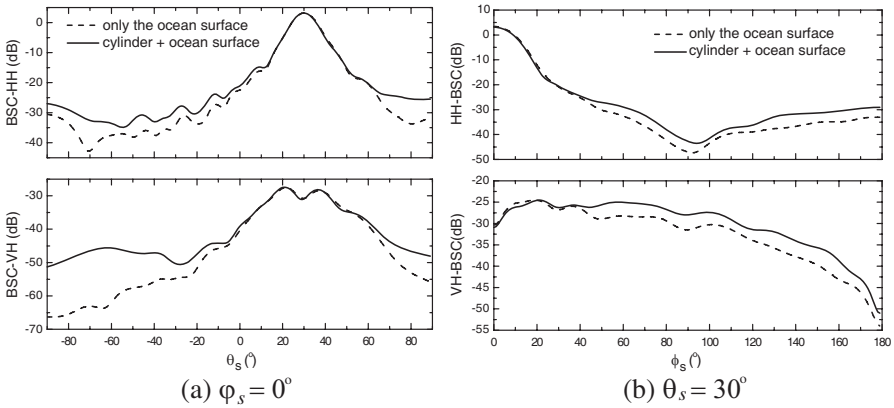

(a) $\varphi_s = 0^o$ (b) $\theta_s = 30^o$

Figure 7. Cylinder partially buried in ocean surface ($\theta_i = 30°$, $\varphi_i = 0°$).

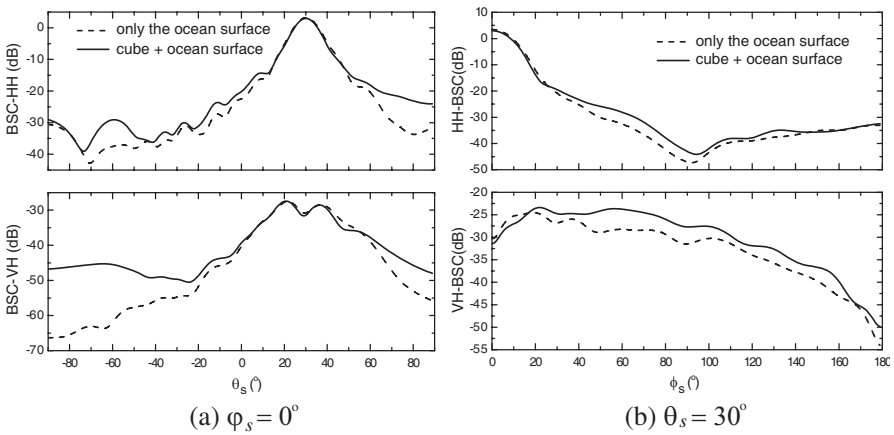

(a) $\varphi_s = 0^o$ (b) $\theta_s = 30^o$

Figure 8. Cube partially buried in ocean surface ($\theta_i = 30°$, $\varphi_i = 0°$).

Figure 9 shows the relative error of unknown induced currents $\tau(n)$ versus iteration steps compared with different objects. It can be seen that, for different objects, the induced currents on the object and rough surface are both convergent after several iteration steps. Experiments show that the G-SMCG method always convergent well for hundreds of realizations. Here we just make the average of 10 realizations, because the computing time will be intolerable if making more realizations. Table 1 shows the computing time for different targets buried in ocean surface. It is clear that the cylinder target requires the most time, due to more iterative steps.

Table 1. Comparison of CPU time for different targets (10 realizations).

Target	CPU time (hours)
Sphere	34.19
Cylinder	48.01
Cube	44.60

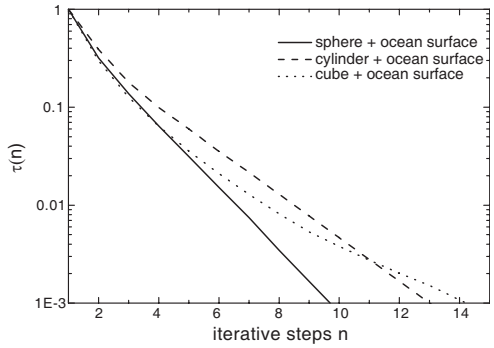

Figure 9. The validation of the computation.

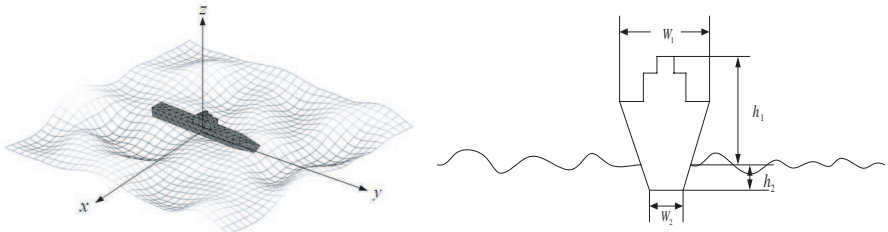

Figure 10. Geometry of a PEC ship located on the ocean surface.

Now, we consider EM scattering from a ship located on the ocean surface as shown in Fig. 10. The length of the ship is 1.8 m. The width of deck is $W_1 = 0.2$ m, and the width of the bilge is $W_2 = 0.14$ m. The height on the ocean surface is $h_1 = 0.15$ m, and the height below the ocean surface is $h_1 = 0.05$ m. The ocean surface and incident wave are the same as those described earlier. The surface of the ship is discretized into 622 triangle patches.

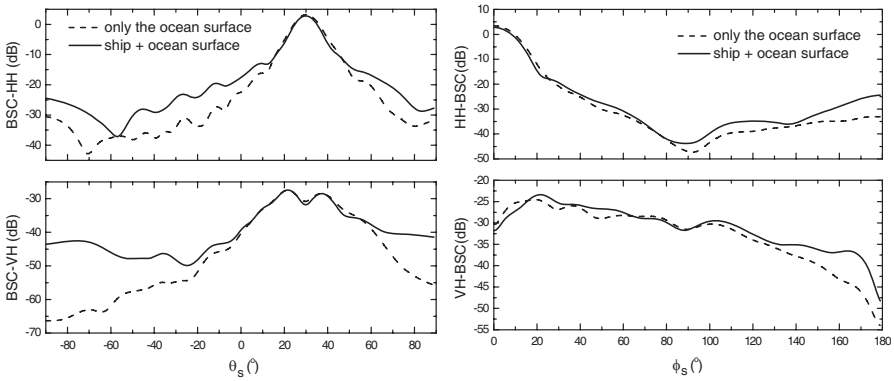

(a) $\varphi_s = 0^\circ$ (b) $\theta_s = 30^\circ$

Figure 11. BSC of ship located on ocean surface ($\theta_i = 30^\circ$, $\varphi_i = 0^\circ$).

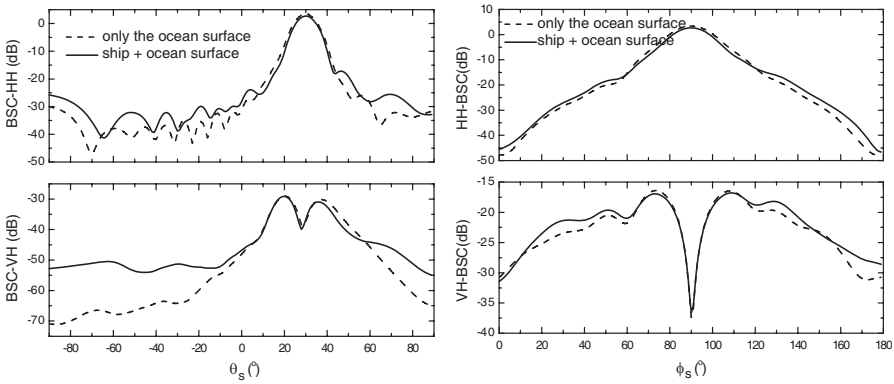

(a) $\varphi_s = 90^\circ$ (b) $\theta_s = 30^\circ$

Figure 12. BSC of ship located on ocean surface ($\theta_i = 30^\circ$, $\varphi_i = 90^\circ$).

Figures 11 and 12 show the BSCs of a ship on the ocean surface. In Fig. 11, the incident azimuth angle is $\varphi_i = 0^\circ$ thus the incident wave irradiates the side face of the ship, and the scattering azimuth angle is $\varphi_s = 0^\circ$. In Fig. 12, the incident azimuth angle is $\varphi_i = 90^\circ$ thus the incident wave irradiates the fore of the ship, and the scattering azimuth angle is $\varphi_s = 90^\circ$. It can be seen that the BSCs are greatly enhanced beyond the specular angle $\theta_s = 30^\circ$, and the changes are more obvious when $\varphi_i = 0^\circ$.

Figure 13 shows the BSCs of the ship located on the ocean surface with different wind speeds, $U_{19.5} = 0\,\mathrm{m/s}$, $U_{19.5} = 3\,\mathrm{m/s}$ and $U_{19.5} = 5\,\mathrm{m/s}$. The other parameters are the same as those used

in Fig. 11. The results show that the BSC decreases as the wind speed decreases. The BSCs of the ship on the ocean surface, as a function of the wind direction ($\phi_v = 30°$, $\phi_v = 50°$ and $\phi_v = 70°$), are shown in Fig. 14. It is observed in Fig. 14(a) that the BSC increases with increasing ϕ_v. The results shown in Fig. 14(b) are interesting. When the azimuth angle is smaller than 90°, the BSC increases with increasing ϕ_v. However, the BSC decreases with increasing ϕ_v when the azimuth angle is bigger than 90°.

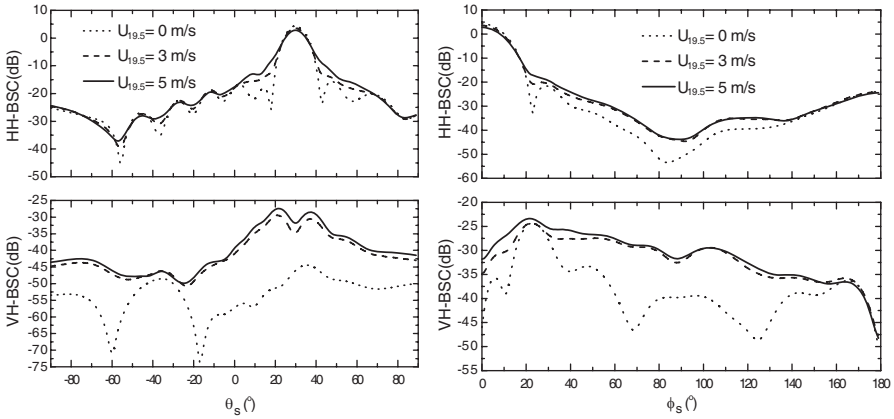

(a) $\varphi_s = 0^o$ (b) $\theta_s = 30^o$

Figure 13. BSC for different wind speed ($\theta_i = 30°$, $\varphi_i = 0°$).

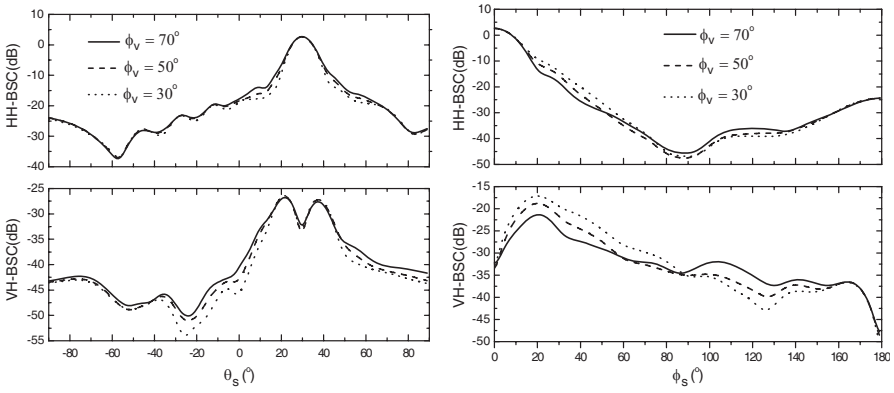

(a) $\varphi_s = 0^o$ (b) $\theta_s = 30^o$

Figure 14. BSC for different wind direction ($\theta_i = 30°$, $\varphi_i = 0°$).

4. CONCLUSION

Based on the sparse matrix canonical grid method (SMCG) and MoM with RWG base function, an efficient approach called general sparse matrix canonical grid method (G-SMCG) is presented. By using this method, arbitrarily shaped PEC 3-D objects partially buried in dielectric 2-D rough surface can be computed quickly. The merit of this method is that the solution accounts for all of the multiple interactions between the rough surface and the object, and the complexity of G-SMCG is similar to SMCG ($O(N \log N)$). It only includes additional cost associated with the direct MoM solution of PEC object.

The EM scattering from typical objects partially buried in ocean surface with PM spectrum are calculated by using G-SMCG, and the accuracy and efficiency of this method are then discussed. The BSCs of ocean surface without object are compared with that of ocean surface with object. The results show that the BSCs are greatly enhanced, and the difference can show the scattering effect due to the object presence. At last, the BSCs of ship located on ocean surface are computed with different incident azimuth angles. The results show that the BSCs are greatly increased due to the ship presence, and the changes are more obvious when the incident wave irradiates the side face of the ship.

ACKNOWLEDGMENT

This work was supported by the State Key Lab. of Millimeter Waves, Nanjing, China (Grant No. K200818, No. K200907). The authors would like to thank the reviewers for their constructive suggestions.

REFERENCES

1. Ye, H. X. and Y. Q. Jin, "Fast iterative approach to difference scattering from the target above a rough surface," *IEEE Trans. on Geoscience and Remote Sensing*, Vol. 44, No. 1, 108–115, 2006.
2. Firoozabadi, R., E. L. Miller, C. M. Rappaport, and A. W. Morgenthaler, "Subsurface sensing of buried objects under a randomly rough surface using scattered electromagnetic field data," *IEEE Trans. on Geoscience and Remote Sensing*, Vol. 45, No. 1, 104–117, 2007.
3. Geng, N., M. A. Ressler, and L. Carin, "Wide-band VHF scattering from a trihedral reflector situated above a lossy dispersive halfspace," *IEEE Trans. on Geoscience and Remote Sensing*, Vol. 27, No. 9, 2609–2617, 1999.

4. Johnson, J. T., "A study of the four-path model for scattering from an object above a halfspace," *Microw. Opt. Technol. Lett.*, Vol. 30, No. 7, 130–134, 2001.
5. Ye, H. X. and Y. Q. Jin, "A hybrid analytical-numerical algorithm for scattering from a 3-D target above a randomly rough surface," *Chin. Phys*, Vol. 57, No. 2, 839–846, 2008.
6. Kuang, L. and Y. Q. Jin, "Bistatic scattering from a three-dimensional object over a randomly rough surface using the FDTD algorithm," *IEEE Trans. Antennas Propagat.*, Vol. 55, No. 8, 1368–1376, 2007.
7. El-Shenawee, M., "The multiple interaction model for non-shallow scatterers buried beneath two-dimensional random rough surfaces," *IEEE Trans. on Geoscience and Remote Sensing*, Vol. 40, No. 4, 982–987, 2002.
8. Liu, Z. J., J. Q. He, Y. J. Xie, A. Sullivan, and L. Carin, "Multilevel fast multipole algorithm for general targets on a half-space interface," *IEEE Trans. Antennas Propagat.*, Vol. 50, No. 12, 1838–1849, 2002.
9. Guan, B., J. F. Zhang, X. Y. Zhou, and T. J. Cui, "Electromagnetic scattering from objects above a rough surface using the method of moments with half-space Green's function," *IEEE. Trans. on Geoscience and Remote Sensing*, Vol. 47, No. 10, 3399–3405, 2009.
10. Lawrence, D. E. and K. Sarabandi, "Electromagnetic scattering from a dielectric cylinder buried beneath a slightly rough surface," *IEEE Trans. Antennas Propagat.*, Vol. 50, No. 10, 1368–1376, 2002.
11. Chiu, T. and K. Scarabandi, "Electromagnetic scattering interaction between a dielectric cylinder and a slightly rough surface," *IEEE Trans. Antennas Propagat.*, Vol. 47, No. 5, 902–913, 1999.
12. Zhang, Y., Y. E. Yang, H. Braunisch, and J. A. Kong, "Electromagnetic wave interaction of conducting object with rough surface by hubrid SPM/MOM technique," *Progress In Electromagnetics Research*, Vol. 22, 315–335, 1999.
13. Wang, X., X. Luo, Z. Zhang, and J. Fu, "The study of an electromagnetic scattering model for two adjacent trunks above a rough surface ground plane," *Microw. Opt. Technol. Lett.*, Vol. 20, No. 6, 369–376, 1999.
14. Wang, Y. H., Y. M. Zhang, and L. X. Guo, "Investigation of the scattered field from a two-dimensional dielectric target above the planar surface with a Guass beam incidence," *Acta Phys.*, Vol. 57,

No. 09, 5529–5536, 2008.

15. Wang, X., C.-F. Wang, Y.-B. Gan, and L.-W. Li, "Electromagnetic scattering from a circular target above or below rough surface," *Progress In Electromagnetics Research*, Vol. 40, 207–227, 2003.
16. Wang, X., Y. B. Gan, and L. W. Li, "Electromagnetic scattering by partially buried PEC cylinder at the dielectric rough surface interface: TM case," *IEEE Antennas and Wireless Propagation Letters*, Vol. 2, 219–322, 2003.
17. Wang, X. and L.-W. Li, "Numerical characterization of bistatic scattering from PEC cylinder partially embedded in a dielectric rough surface interface: Horizontal polarization," *Progress In Electromagnetics Research*, Vol. 91, 35–51, 2009.
18. Wang, X., Y.-B. Gan, and L.-W. Li, "TE scattering from pec object partially embedded at dielectric rtough surface interface," *The Fifth International Kharkov Symposium on Physics and Engineering of Microwaves, Millimeter, and Submillimeter Waves, 2004. MSMW 04*, Vol. 1, 10–26, Kharkov, Ukraine, 2004.
19. Pino, M. P., L. Landesa, J. L. Rodrfguez, F. Obelleiro, and R. J. Burkholder, "The generalized forward-backward method for analyzing the scattering from targets on ocean-like rough surface," *IEEE Trans. Antennas Propagat.*, Vol. 47, No. 6, 961–969, 1999.
20. Li, Z. X., "Bistatic scattering from rough dielectric soil surface with a conducting object partially buried by using the GFBM/SAA method," *IEEE Trans. Antennas Propagat.*, Vol. 54, No. 7, 2072–2080, 2006.
21. Li, Q., L. Tsang, K. S. Pak, and C. H. Chan, "Bistatic scattering and emissivities of random rough dielectric lossy surfaces with the physics-based two-grid method in conjunction with the sparse-matrix canonical grid method," *IEEE Trans. Antennas Propagat.*, Vol. 48, No. 1, 1–11, 2000.
22. Tsang, L., J. A. Kong, and K. H. Ding, *Scattering of Electromagnetic Waves: Numerical Simulations*, New York, 2000.
23. Du, Y., Y. L. Luo, and J. A. Kong, "Electromagnetic scattering from randomly rough surfaces using the stochastic second-degree method and the sparse Matrix/Canonical grid algorithm," *IEEE Trans. Geoscience Remote Sensing*, Vol. 46, No. 10, 2831–2839, 2008.
24. Barrowes, B. E., O. A. Chi, F. L. Teixeira, and J. A. Kong, "Sparse Matrix/Canonical grid method applied to 3-D dense medium simulations," *IEEE Trans. Antennas Propagat.*, Vol. 51, No. 1, 48–58, 2003.

25. Huang, C. C., L. Tsang, C. H. Chan, and K. H. Ding, "Multiple scattering among vias in planar waveguides using preconditioned SMCG method," *IEEE Trans. Microwave Theory Techniques*, Vol. 52, No. 1, 20–28, 2004.
26. Rao, S. M., D. R. Wlton, and A. W. Glisson, "Electromagnetic scattering by surfaces of arbitrary shape," *IEEE Trans. Antennas Propagat.*, Vol. 32, 409–418. 1982.
27. ToPorkov, J. V. and G. S., Brown, "Numerieal simulations of scattering from time-varyingrandomly rough surfaees," *IEEE Trans. Geoscience Remote Sensing*, Vol. 38, No. 4, 1616–1625, 2000.